Journal of Materials Chemistry C

Accepted Manuscript

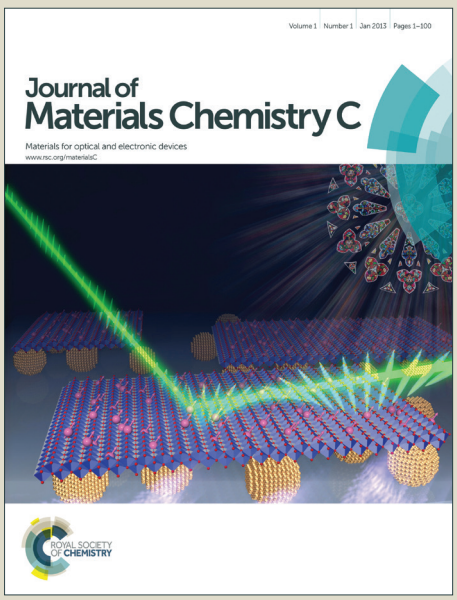

ROYAL SOCIETY OF CHEMISTRY

www.rsc.org/materialsC

ARTICLE TYPE www. rsc.org/xxxxxx | XXXXXXXX

The electronic and magnetic properties of transition-metal elements doped three-dimensional topological Dirac semimetal in Cd_3As_2

Hao Jin,[a,b] Ying Dai,*[a] Yan-Dong Ma,[a] Xin-Ru Li,[a] Wei Wei,[a] Lin Yu, [a] and Bai-Biao Huang[a]

Received Xth XXXXXXXXXX 20XX, Accepted Xth XXXXXXXXX 20XX
First published on the web Xth XXXXXXXXXX 200X
DOI: 10.1039/b000000x

A three-dimensional (3D) topological Dirac semimetal (TDSM) Cd_3As_2 has very recently been discovered, which can be turned into a variety of quantum phases by breaking either time reversal symmetry or inversion symmetry. Here, we present a density functional theory (DFT) study to systematically investigate the doping effects of 3*d* transition-metal (TM) atoms (Ti:Cu) in Cd_3As_2. The results reveal that the introduced 3*d* TMs lower the symmetries of the system, resulting in a massive Dirac fermions with gap opening at the Dirac point. The substitution of Cr atom could tailor Cd_3As_2 to a ferromagnetic half-metal due to the effective *p-d* exchange. The Monte Carlo simulations predict that the Curie temperature (T_c) of Cr-Cd_3As_2 is up to the room temperature, suggesting powerful potentials for further spintronic applications.

1 Introduction

Three-dimensional Dirac topological semimetals (3D-TDSMs) are new class of materials, which has attracted increasing attention in physics and materials science.[1,2] In analogy to 2D graphene, a 3D-TDSM possesses bulk Dirac fermions that disperse linearly along all three momentum directions, which leads to peculiar and novel physical properties, such as unusual electrical and thermal transport,[3] high-temperature linear quantum magnetoresistance,[4] and oscillating quantum spin Hall effect.[2,5] A number of materials and systems have been proposed for realizing the 3D-TDSMs, e.g. $Y_2Ir_2O_7$,[1] β-cristobalite BiO_2,[6] and A_3Bi (A=Na, K, Rb).[2,7] However, these materials are either metastable or difficult to synthesize. As a result, few has been materialized so far. Recently, using first-principle calculations Wang *et al.* predicted a new 3D-TDSMs, i.e. Cd_3As_2,[8] and soon its 3D Dirac cones are experimentally observed.[9–12] In addition, unlike previous 3D-TDSMs, Cd_3As_2 is chemical stable in the air with a remarkably high carrier mobility, which enables it to be a promising candidate in device applications.[13]

Previous studies predict that Cd_3As_2 can be turned into a variety of quantum phases by breaking either time reversal symmetry or inversion symmetry.[8,12] Similar to diluted magnetic semiconductors (DMSs) and 2D Dirac materials, the natural strategy to realize turning effect in Cd_3As_2 is via chemical doping.[14–16] However, to the best of our knowledge, no work has been done to investigate the doping induced phase transformation in Cd_3As_2. In this work, we probe this question by studying the transition metal (TM) atoms in Cd_3As_2 on the basis of density functional theory (DFT) calculations. The stability, electronic and magnetic properties of 3*d* TM atom (Ti:Cu) doped 3D-TDSM Cd_3As_2 are studied in details. In addition, to explore the magnetic coupling, Monte Carlo simulations based on the Ising model are employed and the Curie temperature (T_c) is also estimated.

2 Computational methods

Our spin-polarized DFT calculations were carried out using the Vienna *ab initio* simulation package (VASP),[17,18] with projector augmented wave (PAW) method,[19] and the Perdew-Burke-Ernzerhof (PBE) generalized gradient approximation (GGA) to the exchange correlation functional.[20] A cutoff energy of 500 eV was used to truncate the plane-wave expansion of the wave functions. The strong-correlated correction is considered with GGA+U method to deal with the 3*d*-electrons of TMs.[21] The effective onsite Coulomb interaction parameter (U) and exchange interaction parameter (J) are set to be 4.0 and 0.9 eV, respectively, which are the typical values for 3*d* TMs.[22,23] We also performed calculations with U ranging from 2 eV to 6 eV. The results are comparable to those with U=4 eV, consisted with previous findings (see ESI for details).[16,24] The calculations were performed using a $10\times10\times6$ Monkhorst-Pack *k*-point mesh.[25] In this work, the spin-orbit coupling (SOC) was taken into account by the second variational method on a fully self-consistent basis. Note that the SOC interactions are only included in the band structure calculations, while all the other calculations (e.g. density of states

† Electronic Supplementary Information (ESI) available:. See DOI:

[a] *School of Physics, State Key Laboratory of Crystal Materials, Jinan, 250100, People's Republic of China. E-mail: daiy60@sina.com*
[b] *Department of Materials Engineering, The University of British Columbia, Vancouver, BC, Canada V6T 1Z4*

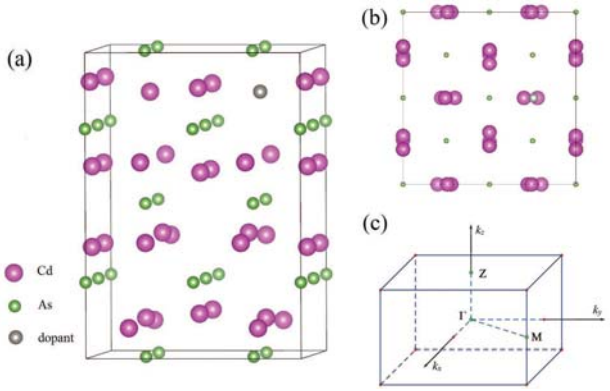

Fig. 1 Crystal structure of Cd_3As_2 with $P4_2/nmc$ symmetry. (a) side view, (b) top view, and (c) Brillouin zone with high symmetric points.

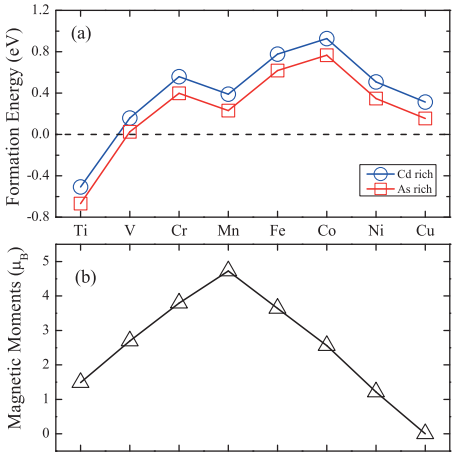

Fig. 2 (a) Calculated formation energies of the most stable configurations of single TM atom doped Cd_3As_2 under different growth conditions, and (b) magnetic moments of TM elements in Cd_3As_2.

calculations) are carried out using spin-polarized calculations without SOC interactions.

A crystallographic cell of Cd_3As_2 is shown in Figure 1, which is related to tetragonally-distorted anti-fluorite structure with Cd in tetrahedral coordination and ordered Cd vacancies.[9,10] The bulk Cd_3As_2 was examined by using a primitive unit cell containing 24 Cd and 16 As atoms, which has D_{4h}^{15} (space group $P4_2/nmc$) symmetry with lattice constants: $a = 8.95$ Å and $c = 12.65$ Å.[9,26] Several test calculations for an 80-atom ($1\times1\times2$ and $2\times1\times1$) supercell gave essentially the same results. The atomic positions were fully relaxed in all reported calculations using the conjugate gradient (CG) method to an energy convergence of 10^{-5} eV and force convergence of 10^{-2} eV/Å.

3 Results and Discussion

We first examine the site preference of a serial of single 3*d* TM impurities. In the calculations, one Cd atom is replaced by the TM atom. The formation energies are computed using the following expression:[27]

$$E_f = E_{tot}(TM) - E_{tot}(bulk) - \sum_i \Delta n_i \mu_i \qquad (1)$$

where $E_{tot}(TM)$ and $E_{tot}(bulk)$ are the total energies of the system with and without TMs. Δn_i indicates the corresponding number that have been added to or removed from the supercell, and μ_i is the chemical potential for species i (host atoms or dopants). We choose hcp Ti, bcc V, bcc Cr, fcc Mn, bcc Fe, fcc Co, fcc Ni, and fcc Cu as reference to evaluate the chemical potentials of these elements. Note that the formation energy is not fixed but depends on the growth conditions, which can be either As-rich or Cd-rich. Under the As-rich condition, μ_{As} is taken as the value of the stable As crystal, whereas μ_{Cd} is calculated by the growth condition:[28]

$$3\mu_{Cd} + 2\mu_{As} = \mu(Cd_3As_2) \qquad (2)$$

Under the Cd-rich condition, μ_{Cd} equals to the value of bulk Cd, whereas the chemical potential of As is calculated via Equation 2. The chemical potential of Cd is in the range of -0.9∼-1.1 eV under different grow conditions, which leads to small difference of formation energy between Cd-rich and Cd-poor conditions. The calculated formation energies of the most stable configurations of single TM doped Cd_3As_2 is shown in Figure 2a. One can see that there is a distinct correlation between the formation energy and impurity size, i.e. E_f decrease with the atomic radius of the impurity. Evidently, for small solutes, such as Fe, Co, etc. the elastic strains induced by the substitutional impurities are considerable large, which introduce large lattice distortions and hence exhibit high formation energies. In contrast, impurities whose size is close to that of Cd exhibit much smaller formation energies. For Ti, negative formation energies are observed under both growth conditions, suggesting that Ti can be spontaneously introduced into Cd_3As_2. Similar size dependent trends were also reported for TM doping in topological insulators, e.g. Bi_2Se_3.[16]

As shown in Figure 2b, the magnetic moments of the TMs with single-filled *d*-states (i.e. Ti, V, Cr, and Mn) increase linearly. While the values decrease linearly for the late TMs (i.e. Fe, Co, Ni, and Cu). This can be qualitatively explained based on the valence electron configuration of the TMs. It is known that a *d*-element has five localized *d*-orbitals. For early TMs, i.e. Ti, V, Cr, and Mn, they have 2, 3, 4, and 5 *d*-electrons, respectively. Due to the large separation between TM and As

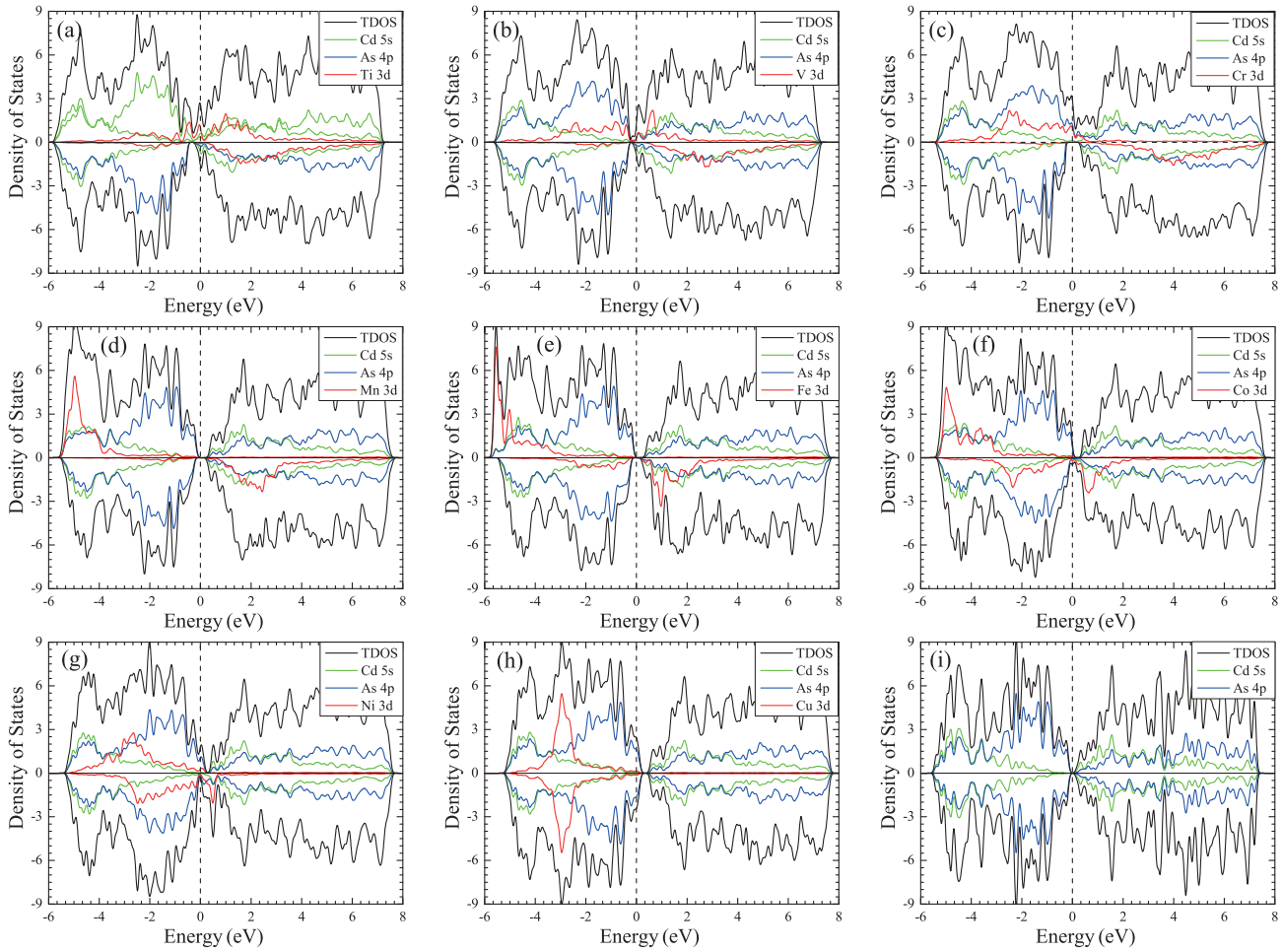

Fig. 3 Total density of states (TDOS) and partial density of states (PDOS) of (a) Ti-, (b) V-, (c) Cr-, (d) Mn-, (e) Fe-, (f) Co, (g) Ni, (h) Cu-doped, and (i) pure Cd_3As_2. The Fermi level is indicated by the dashed line.

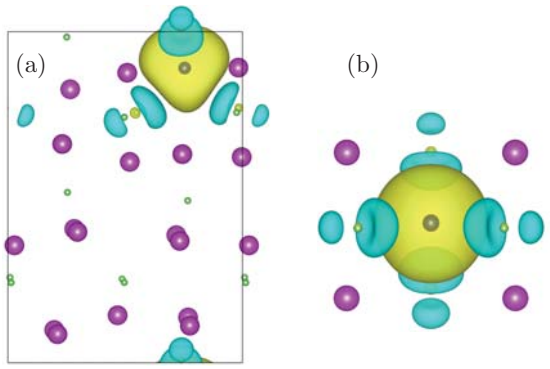

Fig. 4 Isosurface of the magnetization densities ($\rho\uparrow - \rho\downarrow$) of Cr-doped Cd_3As_2 with the isosurface value of 0.002 e/Å^3. (a) Side view, and (b) top view.

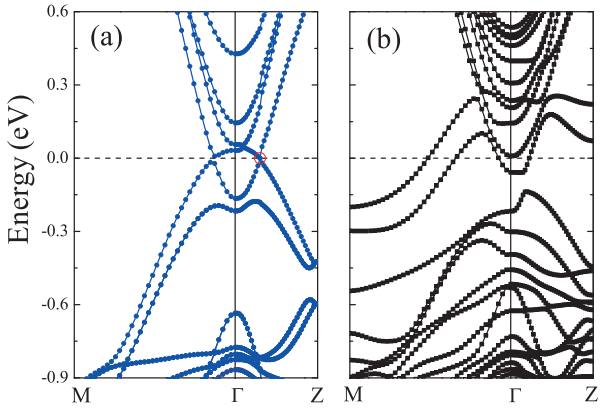

Fig. 5 The calculated band structures of (a) pristine Cd_3As_2, and (b) Cr-doped Cd_3As_2 with SOC. The dashed line indicates the Fermi level. The Dirac point is highlighted by red circle.

atoms, these *d*-electrons are mostly localized and go to separate nonbonding orbitals according to the Hund's rule, which give rise to M=2, 3, 4, and 5μ_B. Especially, for Mn, its unique d^5 configuration yields to the highest spin states among all investigated TMs. The situation changes when the TM atom has more than 5 electrons so that some of the nonbonding orbitals are filled. The magnetic moments go down linearly after Mn. For Cu, all of the *d*-bands are fully occupied and the system is nonmagnetic.

In order to understand the electronic and magnetic structures of all these systems, we analyzed the density of states (DOS) and the band structures of the TM-Cd_3As_2 system. The results are shown in Figure 3. It is seen that Cr doping turns the semi-metallic Cd_3As_2 into a half-metallic material. The spin-down channel (minority states) of the Cr-Cd_3As_2 system is semiconducting with a direct band gap of ∼0.4 eV, whereas the spin-up channel (majority states) shows metallic behavior. Detailed analyses suggest that bands in the vicinity of Fermi level are mainly derived from the hybridization of Cr 3*d* orbitals and the As 4*p* states. Hence, the Cr-Cd_3As_2 system is half-metallic with 100% spin polarization around the Fermi level, which can be quite important for potential use in spintronics. The analysis of magnetization densities ($\rho\uparrow - \rho\downarrow$) indicate that the total magnetic moment of the system comes mostly from the metal atom and partly from its neighboring As atoms, as shown in Figure 4.

For the case of Ti- and V-doped Cd_3As_2, the systems show metallic behaviors. The Fermi level is shifted to the conduction band in both spin-up and spin-down states due to the extra unoccupied *d*-orbitals as compared with the Cr-doped case. The situations are changed when Mn or Fe is introduced into the system. In these cases, the spin-up states of *d*-orbitals are fully occupied and thereby move to the deep range of the valance band, which give rise to semiconducting behavior with a band gap of about 0.4 eV and 0.3 eV for Mn- and Fe-doped cases, respectively. As the elements have more *d*-electrons, the Coulomb interaction gives rise to a shift of the impurity states or/and opening of a gap at the Fermi level.[14] Both the doping of Co and Ni result in metallic ground state, whereas for the case of Cu, the system becomes semiconductor with the band gap of about 0.3 eV.

The calculated band structure of pristine Cd_3As_2 is shown in Figure 5a. In agreement with previous studies,[8,11] the bands cross between Γ and *Z* exactly at the Fermi level. Since both time-reversal and inversion symmetries are present, all bands are doubly degenerate at all momenta in the Brillouin zone, as follows from the Kramers theorem. As a result, there is 4-fold degeneracy at each Fermi point, around which the band dispersions can be linearized. In addition, unlike graphene, the 3D massless Dirac fermions in Cd_3As_2 are robust against the spin-orbit interaction. Previous studies found that Cd_3As_2 is a symmetry-protected 3D TDSM.[8,9,11] If one As atom is replaced by the impurity, the 4-fold rotational symmetry is broken. Recent theoretical studies point out that in this case, a linear leading order term will be introduced in the effective Hamiltonian.[2,8] The massless Dirac fermions will become massive fermions, leading to the opening of an energy gap at the Dirac point. This is indeed the case in our calculations. Compared with the pristine Cd_3As_2, an obvious change of band structure occurs. As shown in Figure 5b through the example of Cr, a band gap of ∼0.1 eV is induced at the Dirac point, which demonstrate the breakdown of the 3D-TDSM state.

As has been discussed above, Cr-doped Cd_3As_2 system shows half-metallic behavior. To investigate the nature of spin exchange coupling, we calculated the exchange energy (E_{ex})

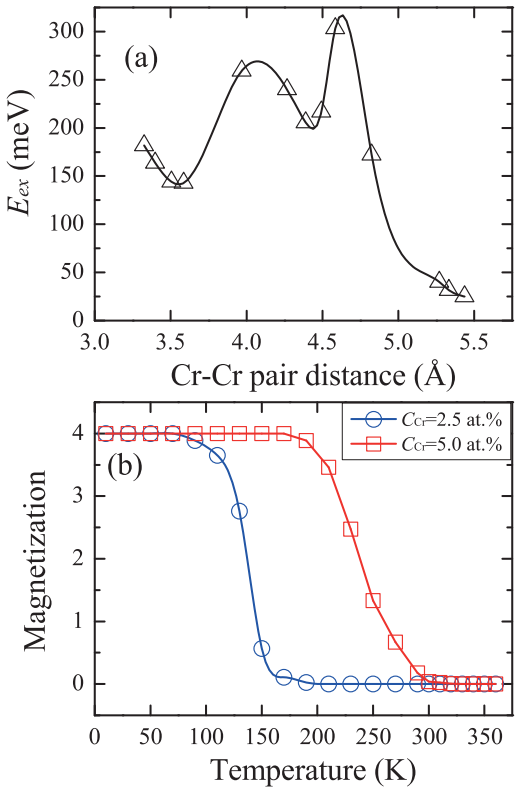

Fig. 6 (a) Calculated exchange energies (E_{ex}) between two substitutional Cr atoms as a function of Cr pair distance. (b) Predicted temperature dependence of the total magnetic moment per unit cell with the Cr concentration of 2.5 at.% and 5.0 at.%, respectively.

by using a 1×1×2 supercell. E_{ex} is estimated by placing two TM dopants in the supercell at various separation distances and comparing the total energy difference between antiferromagnetic (AFM) and FM states of the dopants at the same distance. All possible configurations within 5.5 Å Cr-Cr distance are considered. The results are plotted in Figure 6a. We found that Cr-doped Cd_3As_2 systems possess robust FM ground state with large values of exchange energies (over 300 meV per supercell). This can be understood by checking the electronic structures as shown in Figure 3c, where the conductive *d*-states provide channels for effective coupling via *d*-*p* exchange with the host As atoms.

For further applications such as in spintronic devices, it is important to get a more in-depth understanding especially of the changes in magnetism with temperature. Here, we adopt the Ising model combined with Monte Carlo (MC) simulations to estimate T_c of the Cr-doped Cd_3As_2.[23,29] The Ising Hamiltonian of the system can be described as:

$$H = -\sum_{i,j} J_{ij} m_i m_j \quad (3)$$

where m_i and m_j are the magnetic moments at sites i and j, and J_{ij} is is the exchange coupling constant between the i^{th} and j^{th} Cr atoms, taken from the DFT calculations as shown in Figure 6a. The MC simulations are carried out using a 10×10×10 supercell with periodic boundary conditions. The calculations last for 8×10^6 loops. In each loop, the spins on all the magnetic sites flip randomly (see ESI for details). Larger supercells or longer loops have been tested to give very similar results. From Figure 6b, it can be seen that for $Cd_{2.875}Cr_{0.125}As_2$, the magnetization starts dropping at 100K, and then the paramagnetic (PM) state is obtained at a temperature of about 150K (Curie temperature). For $Cd_{2.75}Cr_{0.25}As_2$, we found that T_c could be up to the room temperature.

4 Conclusions

In summary, we have systematically studied the effects of a series of 3*d* TMs atoms doping in the symmetry-protected 3D TDSM system using DFT calculations. Our work shows that the introduced 3*d* TMs lower the symmetries of the system, resulting in a massive Dirac fermions with gap opening. In addition, 3*d* TMs could turn the semi-metallic Cd_3As_2 into semiconductor, metal, or half-metal. Further calculations indicate that the magnetic coupling between Cr pair in Cd_3As_2 is FM due to the effective *p*-*d* exchange. Using Monte Carlo simulation based on the Ising model, we predict that the Curie temperature of $Cd_{2.75}Cr_{0.25}As_2$ is up to room temperature, suggesting powerful potentials for further spintronic applications.

Acknowledgements

This work is supported by the National Basic Research Program of China (973 program, 2013CB632401), National Natural Science foundation of China under Grants 21333006 and 11174180, the Fund for Doctoral Program of National Education 20120131110066, 111 Project B13029, National Science foundation of China under Grant 11404187, and Natural Science Foundation of Shandong Province under Grant number ZR2013AM021. We thank W. Fan, C. Niu, and J. Lu for stimulating discussions.

References

1 X. Wan, A. M. Turner, A. Vishwanath and S. Y. Savrasov, *Phys. Rev. B*, 2011, **83**, 205101.

2 Z. Wang, Y. Sun, X.-Q. Chen, C. Franchini, G. Xu, H. Weng, X. Dai and Z. Fang, *Phys. Rev. B*, 2012, **85**, 195320.

3 L. Li, J. G. Checkelsky, Y. S. Hor, C. Uher, A. F. Hebard, R. J. Cava and N. P. Ong, *Science*, 2008, **321**, 547–550.

4 W. Zhang, R. Yu, W. Feng, Y. Yao, H. Weng, X. Dai and Z. Fang, *Phys. Rev. Lett.*, 2011, **106**, 156808.

5 C.-X. Liu, H. Zhang, B. Yan, X.-L. Qi, T. Frauenheim, X. Dai, Z. Fang and S.-C. Zhang, *Phys. Rev. B*, 2010, **81**, 041307.

6 S. M. Young, S. Zaheer, J. C. Y. Teo, C. L. Kane, E. J. Mele and A. M. Rappe, *Phys. Rev. Lett.*, 2012, **108**, 140405.

7 Z. K. Liu, B. Zhou, Y. Zhang, Z. J. Wang, H. M. Weng, D. Prabhakaran, S.-K. Mo, Z. X. Shen, Z. Fang, X. Dai, Z. Hussain and Y. L. Chen, *Science*, 2014, **343**, 864–867.

8 Z. Wang, H. Weng, Q. Wu, X. Dai and Z. Fang, *Phys. Rev. B*, 2013, **88**, 125427.

9 M. N. Ali, Q. Gibson, S. Jeon, B. B. Zhou, A. Yazdani and R. J. Cava, *Inorg. Chem.*, 2014, **53**, 4062–4067.

10 S. Borisenko, Q. Gibson, D. Evtushinsky, V. Zabolotnyy, B. Büchner and R. J. Cava, *Phys. Rev. Lett.*, 2014, **113**, 027603.

11 M. Neupane, S.-Y. Xu, R. Sankar, N. Alidoust, G. Bian, C. Liu, I. Belopolski, T.-R. Chang, H.-T. Jeng, H. Lin, A. Bansil, F. Chou and M. Z. Hasan, *Nat. Commun.*, 2014, **5**, 4786.

12 Z. K. Liu, J. Jiang, B. Zhou, Z. J. Wang, Y. Zhang, H. M. Weng, D. Prabhakaran, S. K. Mo, H. Peng, P. Dudin, T. Kim, M. Hoesch, Z. Fang, X. Dai, Z. X. Shen, D. L. Feng, Z. Hussain and Y. L. Chen, *Nat. Mater.*, 2014, **13**, 677–681.

13 W. Zdanowicz and L. Zdanowicz, *Annu. Rev. Mater. Sci.*, 1975, **5**, 301–328.

14 A. V. Krasheninnikov, P. O. Lehtinen, A. S. Foster, P. Pyykkö and R. M. Nieminen, *Phys. Rev. Lett.*, 2009, **102**, 126807.

15 H. Jin, Y. Dai, B.-B. Huang and M.-H. Whangbo, *Appl. Phys. Lett.*, 2009, **94**, 162505.

16 J.-M. Zhang, W. Zhu, Y. Zhang, D. Xiao and Y. Yao, *Phys. Rev. Lett.*, 2012, **109**, 266405.

17 G. Kresse and J. Furthmüller, *Phys. Rev. B*, 1996, **54**, 11169–11186.

18 G. Kresse and J. Furthmüller, *Comput. Mater. Sci.*, 1996, **6**, 15 – 50.

19 G. Kresse and D. Joubert, *Phys. Rev. B*, 1999, **59**, 1758–1775.

20 J. P. Perdew, K. Burke and M. Ernzerhof, *Phys. Rev. Lett.*, 1996, **77**, 3865–3868.

21 A. I. Liechtenstein, V. I. Anisimov and J. Zaanen, *Phys. Rev. B*, 1995, **52**, R5467–R5470.

22 T. O. Wehling, A. I. Lichtenstein and M. I. Katsnelson, *Phys. Rev. B*, 2011, **84**, 235110.

23 X.-X. Li, X.-J. Wu and J.-L. Yang, *J. Am. Chem. Soc.*, 2014, **136**, 5664–5669.

24 J. Zhou and Q. Sun, *J. Am. Chem. Soc.*, 2011, **133**, 15113–15119.

25 H. J. Monkhorst and J. D. Pack, *Phys. Rev. B*, 1976, **13**, 5188–5192.

26 R. Z. Stackelberg, M.; Paulus, *Phys. Chem.*, 1935, **28B**, 427.

27 C.-W. Niu, Y. Dai, Y.-T. Zhu, Y.-D. Ma, L. Yu, S.-H. Han and B.-B. Huang, *Sci. Rep.*, 2012, **2**, 976.

28 H. Jin, Y. Dai, W. Wei and B.-B. Huang, *J. Phys. D: Appl. Phys.*, 2008, **41**, 195411.

29 X. Li, Y. Dai, Y.-D. Ma and B.-B. Huang, *Phys. Chem. Chem. Phys.*, 2014, **16**, 13383–13389.

ARTICLE TYPE www. rsc.org/xxxxxx | XXXXXXXX

Graphical Abstract for Table of Contents

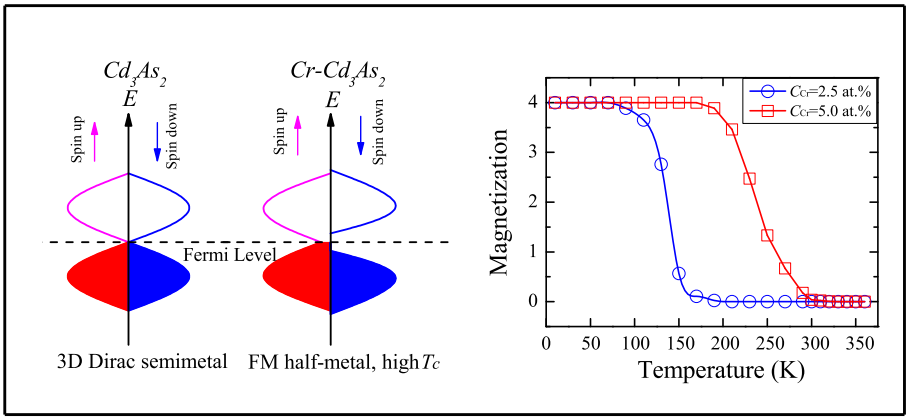

The substitution of Cr atom could tailor Cd_3As_2 to a ferromagnetic half-metal, with the Curie temperature (T_c) up to the room temperature, suggesting powerful potentials for further spintronic applications.